BIOCHEMISTRY
including biophysical chemistry & molecular biology

ARTICLE

pubs.acs.org/biochemistry

The Accumulation of the Light-Harvesting 2 Complex during Remodeling of the *Rhodobacter sphaeroides* Intracytoplasmic Membrane Results in a Slowing of the Electron Transfer Turnover Rate of Photochemical Reaction Centers

Kamil Woronowicz, Daniel Sha, Raoul N. Frese,[†] and Robert A. Niederman*

Department of Molecular Biology and Biochemistry, Rutgers University, Busch Campus, 604 Allison Road, Piscataway, New Jersey 08854-8082, United States

Supporting Information

ABSTRACT: A functional proteomic analysis of the intracytoplasmic membrane (ICM) development process was performed in *Rhodobacter sphaeroides* during adaptation from high-intensity illumination to indirect diffuse light. This initiated an accelerated synthesis of the peripheral light-harvesting 2 (LH2) complex relative to that of LH1−reaction center (RC) core particles. After 11 days, ICM vesicles (chromatophores) and membrane invagination sites were isolated by rate-zone sedimentation and subjected to clear native gel electrophoresis. Proteomic analysis of gel bands containing the RC−LH1 and −LH2 complexes from digitonin-solubilized chromatophores revealed high levels of comigrating electron transfer enzymes, transport proteins, and membrane assembly factors relative to their equivalent gel bands from cells undergoing adaptation to direct low-level illumination. The GroEL chaperonin accounted for >65% of the spectral counts in the RC−LH1 band from membrane invagination sites, which together with the appearance of a universal stress protein suggested that the viability of these cells was challenged by light limitation. Functional aspects of the photosynthetic unit assembly process were monitored by near-IR fast repetition rate analysis of variable fluorescence arising from LH−bacteriochlorophyll *a* components. The quantum yield of the primary charge separation during the early stages of adaptation showed a gradual increase (variable/maximal fluorescence = 0.78−0.83 between 0 and 4 h), while the initial value of ∼70 for the functional absorption cross section (σ) gradually increased to 130 over 4 days. These dramatic σ increases showed a direct relation to gradual slowing of the RC electron transport turnover rate (τ_{QA}) from ∼1.6 to 6.4 ms and an ∼3-fold slowing of the rate of reoxidation of the ubiquinone pool. These slowed rates are not due to changes in UQ pool size, suggesting that the relation between increasing σ and τ_{QA} reflects the imposition of constraints upon free diffusion of ubiquinone redox species between the RC and cytochrome bc_1 complex as the membrane bilayer becomes densely packed with LH2 rings.

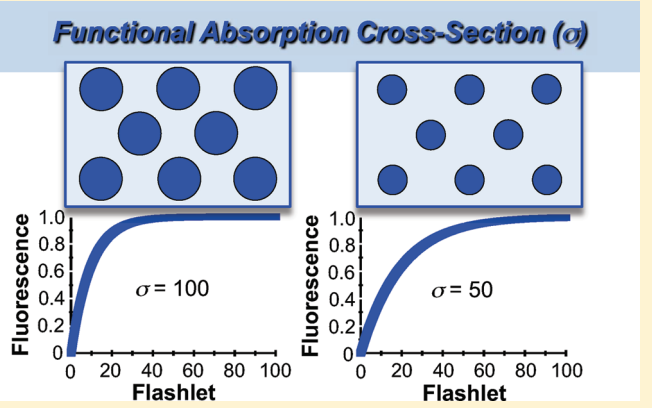

Because of the unparalleled combination of accessible molecular genetics with an intracytoplasmic membrane (ICM) system that is amenable to a considerable variety of biochemical, spectroscopic, and ultrastructural probes, the photosystem[a] of the purple bacterium *Rhodobacter sphaeroides* has served as an important model system for studies of the structural and functional aspects of the light reactions of photosynthesis, as well as related energy transduction processes and the regulatory mechanism controlling the levels of participating protein components.[1] In contrast, much less is known about mechanisms that drive the assembly of the light-harvesting (LH) and reaction center (RC) complexes, how their patterns of localization are established within the cell, and how numerous assembly factors cooperate with the nascent apoproteins and pigments to form functional photosynthetic units within the growing ICM.

The highly detailed picture that we now have for the supramolecular organization of photosynthetic complexes within the *Rba. sphaeroides* ICM[2] also provides a firm basis for studies of energy-transducing membrane assembly in this system. In initial investigations, freeze-fracture transmission electron microscopy (TEM) (reviewed in ref 3), as well as a variety of spectroscopic techniques, provided the principal tools for assessing the distribution of LH and RC components over the surface of the membrane. From the most definitive of these early studies, in which laser-based probes were employed to evaluate singlet−triplet quenching efficiencies in various strains of *Rba. sphaeroides*,[4] it

Received: October 15, 2010
Revised: February 22, 2011
Published: March 02, 2011

was concluded that the core LH1 complex is arranged in clusters that surround and interconnect RCs, with the LH2 antenna positioned peripherally in large lakes. Singlet−singlet annihilation measurements subsequently afforded a quantitative refinement of this proposal, as well as estimates of the size and organization of antenna domains over which excitations can migrate in ICM vesicles (chromatophores).[5−7] In results obtained at 4 K[6] where excitations are thermally restricted to core clusters, an arrangement was proposed in which ∼4 RCs are embedded in core assemblies of ∼100 LH1 BChl molecules, with LH2 BChl molecules interspersed between them, strikingly similar to the organization visualized directly in the subsequent atomic force microscopy (AFM) studies of the *Rba. sphaeroides* ICM.[8−10]

In addition to providing the earliest surface views of intrinsic proteins in a multicomponent energy-transducing membrane system at submolecular resolution, AFM topographs of *Rba. sphaeroides* chromatophores[8] gave a definitive picture of the highly organized arrangement of the RC−LH1 core and LH2 complexes suggested from the exciton annihilation measurements.[7] Two distinct types of domains, composed exclusively of these complexes, were encountered, one with rows of dimeric LH1−RC core structures interspersed with narrow lanes of peripheral LH2 antenna rings and a second one housing closely packed LH2 rings in LH2-only domains, in some cases occupying the entire surface of a vesicle patch. This view of the local intercomplex arrangement has been extended to the long-range organization over the entire surface of oriented chromatophore vesicles by linear dichroism measurements.[11]

Such an arrangement of pigment−protein complexes is optimal for the transfer to LH1of radiant energy harvested by LH2, and the funneling of these excitations to the RC−BChl special pair, where they are transduced into a transmembrane charge separation. This initiates a cycle of electron transfer reactions among the primary iron quinone acceptor (Q_A), the ubiquinol−cytochrome c_2 oxidoreductase (cytochrome bc_1) complex, and cytochrome c_2, resulting in the formation of an electrochemical proton gradient coupled to the synthesis of ATP by an H^+-ATPase of the F_1F_O type.[1] It is noteworthy that in the AFM studies of *Rba. sphaeroides* ICM vesicles, as well as with photosynthetic membranes from a variety of other purple photosynthetic bacteria, neither the cytochrome bc_1 complex nor an F_1F_O-ATPase could be visualized.[8−10]

Under photoheterotrophic growth conditions, cellular levels of the *Rba. sphaeroides* ICM, together with those of LH2 relative to RC−LH1 core complexes, are related inversely to light intensity, thereby permitting the examination of the differential biosynthesis of photosynthetic complexes during the remodeling of the ICM that occurs as cells acclimate from high to lowered illumination levels.[12] Although the formation of an ICM is repressed by high oxygen tension during chemoheterotrophic growth, lowering the oxygen partial pressure initiates a gratuitous induction of ICM assembly in the dark by invagination of the cytoplasmic membrane (CM), together with the synthesis and assembly of LH and RC complexes.[13] In both of these developmental regimens, the sites of CM invagination can be isolated in an upper-pigmented band (UPB), sedimenting more slowly than the ICM-derived chromatophore vesicle fraction during rate-zone sedimentation on sucrose density gradients.[14] Extensive biochemical, biophysical, and ultrastructural characterization of these membrane fractions (reviewed in ref 15) has demonstrated that during induction of ICM synthesis after a switch from high to low levels of aeration, photosynthetic units are assembled sequentially, with RC−LH1 core structures inserted initially into the CM in a form that is largely inactive in forward electron transfer.[13] This is followed by the activation of functional electron flow, together with the addition of LH2, resulting in further invagination and vesicularization of the membrane to form an ICM capable of budding off into discrete membrane vesicles.[16,17] During this developmental process, LH2 is thought to pack initially between linear arrays of dimeric core complexes, and when these regions become filled, the LH2 complex ultimately forms a light-responsive peripheral antenna complement by clustering into LH2-only domains.[18]

In efforts to further elucidate the ICM assembly process, we have initiated a detailed structural and functional proteomic analysis of membrane remodeling in *Rba. sphaeroides* undergoing adaptation to reduced light intensity.[12] Proteomics approaches are focused upon the global identification of proteins that are temporally expressed during ICM induction or remodeling and are spatially localized in both membrane growth initiation sites and mature ICM vesicles. Developmental changes in these distinct proteomes are correlated with AFM topographs to follow how the local organization of membrane protein complexes becomes established at submolecular resolution. As functional correlates of this structural proteomics approach, fast repetition rate (FRR) analysis of fluorescence transients arising from the BChl components of the LH complex is used to monitor increases in the functional absorption section, as well as changes in the quantum yield of the primary charge separation and RC electron transfer turnover rates.

In this investigation, cells grown at a high light intensity were shifted to indirect diffuse illumination in an attempt to obtain maximal increases in the absorption cross section as the levels of ICM increased largely through membrane remodeling as a result of the accelerated synthesis of the LH2 complex. Here, we present a functional proteomic examination of the upper-pigmented and chromatophore fractions isolated after prolonged exposure to diffuse light, coupled with the results of a detailed FRR fluorescence analysis of cells undergoing this ICM remodeling process.

The relevance of the analysis of FRR variable BChl fluorescence transients to the elucidation of the functional aspects of the photosynthetic complex assembly process was previously established in *Rba. sphaeroides* undergoing gratuitous induction of ICM formation at low levels of aeration.[13] As detailed by Kolber et al.,[19] in FRR fluorescence analysis, an initial strong light pulse of short duration elicits a single charge separation in all RCs. The resulting variable fluorescence signal reflects the RC redox status, where a low fluorescence yield indicates an open RC (no charge, ready to perform photochemistry) and a high fluorescence yield indicates a closed RC (photooxidized charged RC, transiently nonfunctional). The difference between the minimal fluorescence (F_0) and maximal fluorescence (F_M) gives an estimate of the quantum yield of the primary charge separation (estimated from the F_V/F_M ratio, where variable fluorescence $F_V = F_M - F_0$). The analysis of the induction kinetics provides estimates of the functional absorption cross section (σ) of the LH complexes, as well as their connectivity (p), as reflected by the sigmoidicity of the fluorescence induction process. The subsequent relaxation kinetics arise from the reopening of the RC as governed by the RC electron transfer turnover rate (τ_{QA}). In this study, FRR fluorometry is used to follow the extensive ICM remodeling process initiated by a switch from high-intensity illumination to a prolonged exposure to indirect diffuse light in an effort to

maximally expand the functional absorption cross section; these increases are then correlated with changes in the other measured FRR parameters and to a proteomic analysis of the final state of both membrane invagination sites and the mature ICM.

MATERIALS AND METHODS

Cell Growth and Membrane Isolation. Using 1 L Roux bottles, *Rba. sphaeroides* wild-type strain NCIB 8253 was grown photoheterotrophically at 30 °C in the medium described by Cohen-Bazire et al.[20] Cells were initially grown at a high light intensity (1100 W/m^2) in a water-cooled plastic aquarium illuminated by two apposed 150 W tungsten lamps controlled by a rheostat. After reaching an OD_{680} of 0.2, cells were transferred to a refrigerated incubator and subjected to weak indirect illumination provided by a 40 W tungsten bulb facing downward at a distance of ~1 m, giving a light intensity at the culture surface of 30 W/m^2. Light intensities were monitored with a YSI-Kettering radiometer. *Rba. sphaeroides* LH2$^-$ strain M21 was grown semiaerobically in Erlenmeyer flasks filled to 80% capacity on a gyratory shaker at 200 rpm and used in the initial experiment. In the next experiment, samples of adapting wild-type cells were taken every 15 min over a 2 h period, while in the final experiment, samples were taken at 10−15 min intervals during the first hour, every 15 min during the second hour, at 3 and 4 h, and thereafter at 3, 4, and 11 days.

The final 11 day sample was pelleted at 11000*g* and 4 °C, washed, and resuspended in 1 mM Tris (pH 7.5); a few crystals of DNaseI (Roche) and protease inhibitor cocktail (Roche) were added, and the cells were passed twice through a French press. Debris and unbroken cells were removed by centrifugation at 12000*g*. The supernatant was layered onto a 5 to 35% (w/w) sucrose gradient prepared over a 60% sucrose cushion and subjected to rate-zone ultracentrifugation for 3 h at 28000 rpm in Beckman SW-28 rotor. Two bands were collected: the UPB, containing membrane growth initiation sites, and the main pigmented band, containing mature chromatophores.

Clear Native Electrophoresis. Chromatophore and UPB samples were solubilized with 2 g of digitonin/g of total protein and applied to a 5 to 10% polyacrylamide clear native gel as described by Wittig et al.[21] Protein concentrations were determined using the BSA protein assay (Thermo), and 312 μg of total protein was loaded onto each lane. Electrophoresis was performed in a Vertical Slab Unit model SE-400 instrument (Hoeffer Scientific Instruments) at 10 mA, until current was no longer measurable. Up to four pigmented bands have previously been identified without staining, and their pigment−protein complex composition was determined from absorption spectra of the excised bands.[12] The gels were scanned using a Canon visible light scanner, before and after they had been stained with Coomassie-based stain (Gel Code blue safe, Thermo).

Proteomic Analysis. Pigmented as well as Commassie-stained gel bands resolved in CNE were excised and fixed for 30 min in a 40% methanol/10% acetic acid solution and subjected to in-gel digestion with trypsin, followed by LC−MS/MS using Thermo LTQ and Dionex U-3000 systems, operated in the nanoLC mode to yield subfemtomole sensitivity.

Fast Repetition Rate Fluorometry. FRR fluorescence signals of the various *Rba. sphaeroides* cell preparations were measured in a Fluorescence Induction and Relaxation (FIRe) system (Satlantic Inc., Halifax, NS). The excitation source consists of a blue LED (450 nm, 30 nm bandwidth), controlled by an LED circuit driver capable of generating pulses with durations of 1 μs to 50 ms. The fluorescence emission is passed through an 880 nm interference filter (50 nm bandwidth) and detected by a sensitive avalanche photodiode module. The digitized fluorescence kinetic transients obtained at 880 nm are processed by computer-assisted analysis, which translates the measured signal into several physiological parameters, following the charge separation elicited between the RC−BChl special pair and the primary quinone electron acceptor (Q_A). These include the functional absorption cross section (σ), the quantum yield of the primary charge separation (F_V/F_M), and the electron transfer turnover rate of the RC (τ_{QA}), which provide the basis for the functional analysis pursued here. F_V/F_M and σ are extracted from the initial rapid phase as described previously,[13] where σ is calculated from the slope of this single-turnover saturation curve and is related to the rate of the increase in fluorescence yield, while the relaxation kinetics are expressed as the RC electron transfer turnover rate (τ_{QA}), because it is uncertain whether this parameter reflects RC−BChl special pair re-reduction or Q_A reoxidation. In our previous study,[13] values obtained for the functional absorption cross section, reflecting the functional antennae size, ranged from 28 to 100 Å^2, roughly corresponding to 32−120 BChl molecules per RC. The functional absorption cross section also depends upon where the excitation wavelength intervenes in the excitation energy transfer pathway (e.g., values obtained with 795 nm excitation directly into the LH2 800 nm band were usually ~1.2-fold greater than those obtained with 470 nm excitation[13]). Accordingly, the functional absorption cross section is expressed here as σ_{450}, the maximal wavelength of the blue LED excitation source (30 nm bandwidth), which excites LH1- and LH2-bound spheroidene and spheroidenone to the $S_2(1Bu^+)$ state, from which excitation energy is transferred to both the Q_X and Q_Y bands of the LH1 and LH2 BChls.[22]

RESULTS

Fast Repetition Rate Fluorescence Analysis Demonstrates a Gradual Slowing of Reaction Center Electron Transfer Turnover Rates in Cells Undergoing ICM Remodeling. FRR transients arising from various *Rba. sphaeroides* cell preparations are shown in Figure 1. While the quantum yield of the primary charge separation was comparable in cells grown at the different light intensities and in the mutant strain lacking LH2 (Table 1), these preparations clearly differ in the rate of rapid fluorescence induction, indicative of the different sizes (σ, functional absorption cross section) of their complement of LH complexes. As expected from the distribution of LH complexes (see below), σ is substantially elevated in the low-light cells, while the σ values are comparable in the LH2-depleted high-light cells and in the LH2$^-$ mutant strain. It is especially noteworthy that a correlation was observed between a slowing of the electron transport turnover rate (τ_{QA}) and the formation of the LH2 antenna during the decrease in light intensity The rate was relatively fast (1.2 ms) during growth at 1100 W/m^2 but decreased to 3.2 ms in the cells adapted to a lower light intensity (100 W/m^2). This is examined in greater detail below in cells adapting from growth at a high light intensity to indirect diffuse illumination for an extended period.

Figure 2 shows the cell density (OD_{680}) profile, the molar LH2:LH1 ratios, and scatter-corrected whole cell spectra during an extended period of adaptation to weak diffuse light conditions in an attempt to significantly expand the functional absorption cross section. One can see from both the increases in the cellular

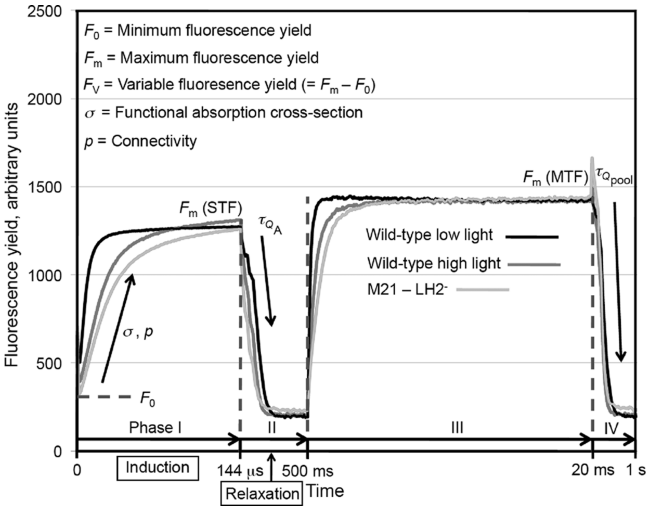

Figure 1. FRR fluorescence kinetic transients elicited upon 450 nm excitation of wild-type *Rba. sphaeroides* grown photoheterotrophically under high (1100 W/m^2) and low (100 W/m^2) light intensities and the LH2$^-$ mutant strain M21 grown semiaerobically. Four phases can be distinguished: phase I, induction phase (strong short pulse with a duration of ~144 μs), resulting in a single-turnover flash (STF), cumulatively saturating the photosystem, permitting measurement of fluorescence induction from F_0 to F_M; phase II, relaxation phase in which indirect modulated light is applied to assess the relaxation kinetics of the fluorescence yield on the 500 ms time scale, reflecting RC reopening; phase III, in which a 20 ms flash induces multiple turnovers saturating the photosystem and UQ pool (MTF, multiple-turnover flash); and phase IV, applying indirect modulated light that records the kinetics of UQ pool reoxidation, using a 1 s time scale. The transients shown here represent signal-averaged sets of 20 traces per sample, which minimized noise levels of individual traces. Note the difference in the rate of fluorescence induction between the wild-type cells grown at low and high light intensities. This reflects the difference in the LH complex cross section (σ); in the latter cells, σ is comparable to that of the LH2-deficient mutant (Table 1). Because the initial fluorescence increase in these transients is nearly exponential, the connectivity (p) between photosynthetic units, derived from the sigmoidicity of the increase, gave low values, ranging from 0.055 at time zero to 0.103 after 11 days.

Table 1. Comparison of Variable Fluorescence Parameters of *Rba. sphaeroides* Cells[a]

cell preparation	F_V/F_M	σ_{450}	p (connectivity)	τ_{QA} (ms)
wild type, high light (1100 W/m^2)	0.77	27	0.15	1.2
wild type, low light (100 W/m^2)	0.76	75	0.06	3.1
strain M21 (LH2$^-$)	0.70	35	0.04	0.7

[a] All values were determined from signal-averaged sets of 20 traces per sample, to minimize the noise levels of individual traces.

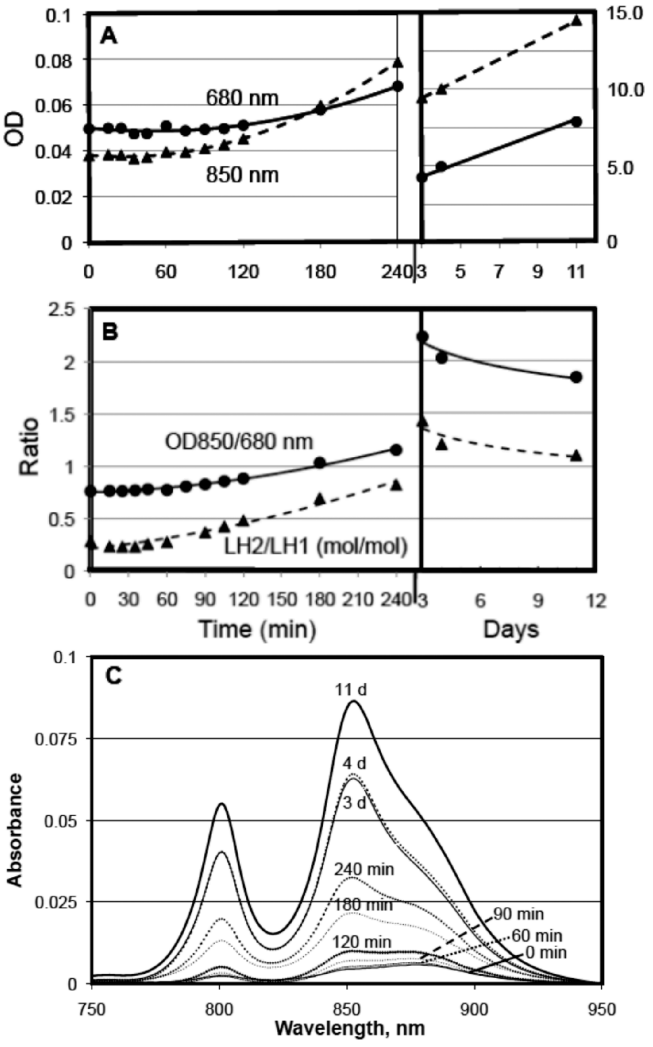

Figure 2. Long-term adaptation of *Rba. sphaeroides* to a shift from high light levels to weak diffuse illumination. (A) Kinetics of increases in cell optical density (680 nm) and accumulation of LH complexes (850 nm). The absolute OD values in the right panel were obtained by appropriate dilutions of the culture. (B) LH2:LH1 molar ratios calculated from whole-cell absorption spectra after correction for light scattering (see panel C). Spectra were recorded with a Beckman DU-640 spectrophotometer, and LH2 and LH1 concentrations were calculated on a BChl basis using the extinction coefficients in ref 23, after deconvolution with the respective band crossover factors. (C) Near-IR absorption spectra of whole cells after correction for light scattering showing growth in the levels of the 800 and 850 nm Q_Y absorption bands (B800 and B850 bands, respectively) of the LH2 peripheral antenna complex; the Q_Y absorption band of the LH1 core antenna complex has a maximum at 875 nm (B875 band).[23]

OD_{850} and the LH2/LH1 ratio of cells sampled over a 4 h period and after 3, 4, and 11 days (panels A and B) that during acclimation to this extreme decrease in illumination level, the synthesis of the LH2 peripheral antenna began to accelerate after a brief lag. The LH2:LH1 ratio reached a value in excess of 1.4 after 3 days and remained at elevated levels thereafter. A gradual increase in the OD_{680} was observed over the entire time course of the experiment, reaching a value of 7.9 at 11 days. This growth yield can be compared to that of cells grown in the absence of photon limitation (e.g., 500 W/m^2), which typically reach an OD_{680} of 17 in fewer than 3 days, showing that the malate electron donor is in excess in the growth medium. This indicates that growth during the light downshift examined here was not nutrient-limited but instead was limited by the weak diffuse illumination. Moreover, a proteomic analysis of the RC−LH1 and LH2-containing CNE gel bands resolved from the chromatophores of cells shifted from 1100 to 100 W/m^2 [12] revealed a protein distribution expected for normal growth conditions and a normal membrane invagination process. In contrast, proteomic analysis of the gel bands from the UPB and chromatophore

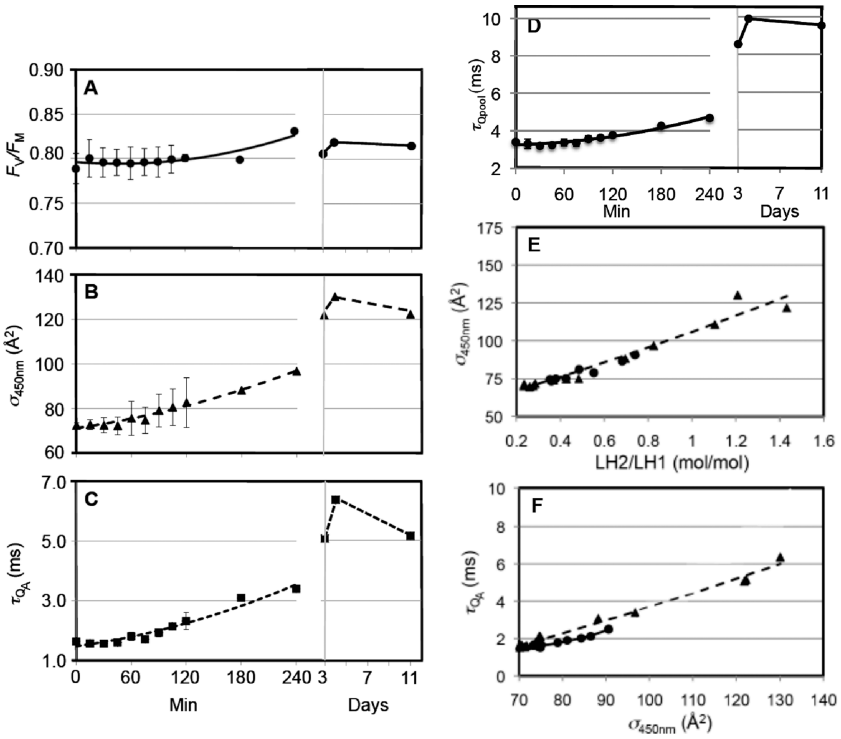

Figure 3. FRR analyses of fluorescence transients of whole cells undergoing a long-term adaptation to a shift from a high light level to weak diffuse illumination. Values were calculated from FRR kinetic transients obtained at 880 nm after excitation at 450 nm; the analyzed transients represented signal-averaged sets of 20 traces per sample, which minimized noise levels in individual traces. (A) Quantum yield of primary charge separation (F_V/F_M) vs adaptation time. Values over the first 2 h in this panel and in panels B−D are averaged with an initial 2 h experiment, which defined the overall trends that were subsequently continued over the extended time course. (B) Functional absorption cross sections (σ_{450}). (C) Reaction center electron transfer turnover rates (τ_{QA}). (D) Rates of reoxidation of the UQ pool (τ_{Qpool}). (E) Functional absorption cross sections (σ_{450}) vs molar LH2:LH1 ratios. (F) Reaction center electron transfer turnover rates (τ_{QA}) vs functional absorption cross sections ($\sigma_{450\ nm}$). In panels E and F, filled circles represent values from the initial 2 h experiment and filled triangles values from the experiment with an extended time course. The lines through the points in panels E and F and over the first 4 h in panels A−D represent polynomial fits. Error bars in panels A−D indicate the standard deviation of measurements from the two different experiments.

fractions of the 11-day-old cells (see below) resulted in the identification of a variety of proteins, indicating that the viability of these cells was challenged by light limitation and that the ICM invagination process had been partially arrested.

The gradual increases in the functional parameters assessed by the FRR fluorescence analysis over the time course of this experiment are shown in Figure 3A−D. The quantum yield of the primary charge separation gradually rose to 0.83 by 4 h but leveled off over the subsequent extended time course (panel A). The σ_{450} values rose markedly during the initial 4 h, ultimately reaching a level of 130 Å^2 by the fourth day (panel B), which represents a near doubling of the functional absorption cross section relative to the value given in Table 1. A gradual slowing of τ_{QA} was observed (panel C), which mirrored the increase in σ, confirming the previous observations in Table 1 and in steady-state cells during adaptation to reduced oxygen tension.[13] This was confirmed in a plot of the rates of reoxidation of UQ pool (τ_{Qpool}), which showed a nearly 3-fold slowing as compared to 4-fold decrease in τ_{QA} over the time course of this experiment. Panel E shows a nearly linear relation between the size of the functional absorption cross section and the LH2:LH1 molar ratios. This relationship is expected because both parameters reflect relative increases in the size of the LH2 antennae per RC, as the size of LH1 per RC remains constant. A plot of the slowing of τ_{QA} versus the rising σ_{450} also shows a rising nearly linear relation (panel F), which apparently reflects a crowding by the LH2 protein as the ICM undergoes remodeling during acclimation to the reduced light intensity, thereby slowing the flow of UQ between the RC and cytochrome bc_1 complexes. This is being examined further by an AFM analysis of the developing ICM and is discussed in detail below.

Proteomic Analysis of Membrane Fractions Isolated from Cells Adapted to Indirect Diffuse Light. To further characterize the process of adaptation to diffuse, indirect illumination and the assembly of the LH2 and RC−LH1 complexes under these conditions, chromatophore and upper-pigmented fractions were isolated at the termination of this experiment and subjected to CNE (Figure 4). The elevated LH2:LH1 molar ratio in chromatophore vesicles (panel A) suggested that the ICM from which they are derived serves as the main site of LH2 accumulation, while the higher relative LH1 level in the UPB confirms that these membranes are derived from preferential sites of assembly of the RC−LH1 complex.[14,15] The availability of both the isolated chromatophore and UPB fractions therefore provided an opportunity to separately examine the membrane domains in which development of photosynthetic complexes is both initiated and completed. By coupling this proteomic study to the FRR fluorescence analysis, we were able to link the observed changes in functional parameters to global protein differences in the distinct membrane domains.

dx.doi.org/10.1021/bi101667e |*Biochemistry* 2011, 50, 4819–4829

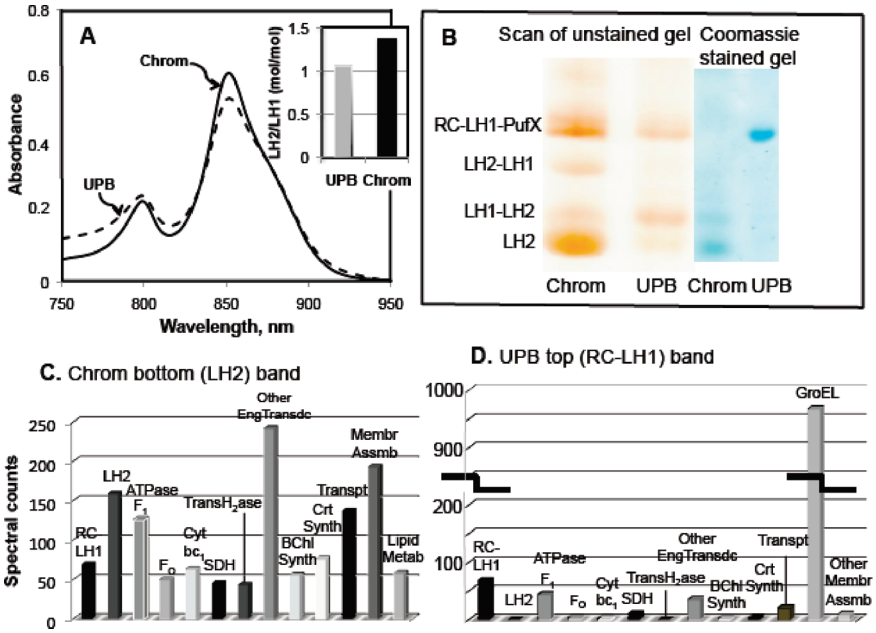

Figure 4. Proteomic analysis of CNE gel bands obtained from upper-pigmented band and chromatophore fractions isolated after an 11 day exposure to diffuse illumination. (A) Near-IR absorption spectra of upper-pigmented band and chromatophore fractions, normalized at 875 nm to illustrate differences in LH2 levels from absorbance of B800 and B850 bands. The inset shows the LH2:LH1 molar ratios. (B) CNE gel separation of intact pigment−protein complexes from UPB and chromatophore fractions solubilized with digitonin (2 g/g of protein) and applied to a 5 to 10% polyacrylamide gradient gel. Bands were identified by absorption spectra obtained directly on gel slices (data not shown). These membrane preparations were from cells adapted to a light intensity of 100 W/m^2 for 24 h; all four bands are seen in chromatophores, while only three appeared in the UPB fraction, with the bottom (LH2) band being significantly lower in abundance than in chromatophores. The chromatophores and UPB from the cells adapted to diffuse illumination (30 W/m^2) are shown in a Coomassie blue-stained gel on the right; bands were excised from the gel and subjected to proteomic analysis after localization of indistinct UPB bands by alignment with those of a typical gel. (C) Proteomic analysis of the chromatophore bottom (LH2) CNE gel band and (D) UPB top band (RC−LH1−PufX complex), showing a distribution of spectral counts for membrane proteins complexes and membrane protein clusters of orthologous groups;[24] note the split in the spectral count scale in panel D. Excised gel bands were subjected to in-gel trypsin digestion and LC−MS/MS as described in Materials and Methods. The constancy and reproducibility of the trypsin proteolysis yields with the different gel bands were demonstrated by comparisons of spectral counts in the LH1-α and LH1-β polypeptides and RC-L, -M, and -H subunits in the chromatophore LH1−LH2 band with the LH1-enriched bands from chromatophores formed under low levels of aeration from the same LC−MS/MS run. The respective RC-M:RC-H and RC-L:RC-H ratios of the chromatophore LH1−LH2 band were 0.50 and 0.10, respectively, while the LH1-β:LH1-α ratio was 0.10; for the low-level aeration preparations, these ratios with the RC−LH1 and LH1−LH2 bands were 0.48 and 0.45, respectively, while the RC-L:RC-H ratio was 0.12 for both bands. The total LH1/RC counts were 0.78 for the diffuse light LH1−LH2 band and 0.65 and 0.69 for the respective induction bands. Spectral counts were too low for such a comparison for the RC−LH1 polypeptides in the UPB gel bands.

The unstained gel shown in Figure 4B was obtained after solubilization of control membranes from cells adapted to a low level of light (100 W/m^2) with the mild detergent digitonin, which gave rise to four bands with both the chromatophore and UPB fractions as opposed to the harsher *n*-octyl β-D-glucopyranoside/deoxycholate mixture used previously,[12] which was only successful with chromatophores. Near-IR and visible absorption spectra obtained directly on excised gel slices demonstrated that the top and bottom bands were essentially spectrally homogeneous, with the top band exhibiting an RC−LH1 spectrum and the bottom one an LH2 spectrum. In contrast, the bands of intermediate migration contained mixtures of these complexes, with the lower intermediate RC−LH1 band enriched (designated as the LH1−LH2 band), while the upper one was LH2-enriched (LH2−LH1 band). These intermediate complexes are thought to represent detergent/protein micelles in which LH2−LH1 associations remain intact and arise from ICM regions where these complexes are in contact, as observed in AFM topographs.[8] It is also noteworthy that the levels of the various bands reflect the relative LH2 and LH1 levels in the original membrane fractions, as demonstrated by the low levels of the bottom LH2 and the upper intermediate LH2−LH1 bands obtained with the LH1-enriched UPB that appear as major bands with the LH2-enriched chromatophores.

Separation of intact pigment−protein complexes from both the chromatophore and UPB fractions by CNE has permitted in-gel trypsin digestion of the pigmented gel bands that were then subjected to LC−MS/MS for proteomic analysis as described in Materials and Methods. It should be emphasized that the proteomics data at this point are expressed in spectral counts, which reflect only the ability of trypsin to act at potential cleavage sites and are therefore of a semiquantitative nature. This means that less abundant proteins with a large number of sites can give larger counts than more abundant proteins with far fewer sites; in cases where no sites are available, no counts are found in the proteomic analysis. Nevertheless, because equal amounts of protein are loaded on each gel lane, valid comparisons can be made between the same components in different gel bands, as well as in designated clusters of orthologous groups[24] into which the proteins are classified (Figure 4C,D). The constancy of the trypsin proteolysis yields is demonstrated by the expected ratios found for the invariant LH1 and RC polypeptides with respect to each other as detailed in the legend of Figure 4.

Although the relative spectral counts arising from proteomic analysis of the LH2 and RC−LH1 complexes in the chromatophore gel bands (Figure 4C and Figure S1A of the Supporting Information) confirmed their distribution as determined in absorption spectra (not shown), they are much less abundant in the LH2 band than previously observed in bands from low-light chromatophores of unstressed cells that had adapted to a light intensity of 100 W/m^2.[12] Accordingly, in the diffuse-light LH2 preparation, LH2 and the RC−LH1 complex represented 9 and 4% of the spectral counts, respectively (Figure S2A of the Supporting Information), while in low-light chromatophores, these values were 30 and 7%, respectively.[12] In contrast, other membrane components were significantly elevated in the diffuse-light and low-light LH2 bands, especially energy transduction-coupled oxidoreductases (14 and 3%, respectively) and transport proteins (8 and 2%, respectively). Because the oxidoreductase and transport proteins are CM components, these comparative distributions would suggest that the CM of diffuse light-adapted cells has invaginated to form ICM to a lesser extent than in the cells adapted to low light levels. The greatly elevated membrane assembly factor accumulation in the diffuse-light vs. low-light LH2 bands (11 and 2%, respectively) reflects the membrane protein distributions in the diffuse-light chromatophores, insofar as assembly of LH2 is greatly outpaced by the formation of factors needed for the active assembly of the elevated levels of the other integral membrane proteins. For the LH1−LH2 band (Figure S2B of the Supporting Information), besides differences in LH2 (3% for diffuse-light vs 10% for low-light chromatophores), the most significant differences were in energy transduction-coupled oxidoreductases (14% for diffuse-light vs 4% for low-light chromatophores), membrane assembly factors (7% vs 3%), transport proteins (5% vs 1%), and succinate dehyrogenase (4% vs 2%).

The distribution of protein clusters arising from the proteomic analysis of all four gel bands from the UPB is shown in Figure 4D and Figure S3A−D of the Supporting Information. Surprisingly, the GroEL chaperonin, comprising 67% of the total spectral counts, was by far the major protein in the RC−LH1 band. This, together with the appearance of a 29.9 kDa universal stress protein (Usp) (see the legend of Figure S1 of the Supporting Information), demonstrates that the viability of the diffuse illumination-exposed cells is challenged under the conditions of light limitation. Other striking observations with the UPB gel bands were the near absence of LH2 spectral counts, the highly elevated GroEL counts (14%) also found in the LH1−LH2 band, and the presence of a high level of translation-associated proteins in this band and in the LH2 and LH2−LH1 bands (18−20%) that were mainly comprised of ribosomal structural proteins. Other soluble proteins consisting of enzymes of amino acid (7−10%) and carbohydrate (11−14%) metabolism were also found at high concentrations in these three bands; these, along with translation proteins, were largely removed from the low-light UPB by a two-phase partitioning procedure.[12] Very high levels of F_1F_O-ATPase (24%) were found in the UPB upper intermediate band (Figure S3B of the Supporting Information), as well as in the other UPB bands and in the chromatophore bands (10% of the total spectral counts in each). The presence in UPB gel bands of considerable spectral counts attributable to oxidoreductases (up to 8%) and transport proteins (up to 9%) is consistent with the origin of this membrane fraction from CM-associated invagination sites. Also noteworthy is the absence of LH2 spectral counts in the UPB gel bands, which can represent 3−5% of the spectral counts in those from the UPB of unstressed cells. This may be related to the possibility that invagination of the ICM has been partially arrested as suggested by the high content of CM markers in chromatophores from the stressed cells. Because LH2 is thought to be a membrane bending protein required for vesicularization of the ICM,[25,26] the limited incorporation of LH2 into the UPB invagination sites may contribute to this apparent defect in the vesicularization process.

DISCUSSION

How Do Ubiquinone Redox Species Diffuse over Large Distances in the ICM Bilayer Congested with Tightly Packed Photosynthetic Complexes? Because of the recent AFM surface views of the native architecture of the ICM of several species of purple photosynthetic bacteria at submolecular resolution (reviewed in refs 9, 10, and 27), renewed interest in possible pathways of UQ diffusion in the ICM bilayer between the RC and cytochrome bc_1 complexes has arisen. While highly organized arrangements of LH2 and RC−LH1 complexes were observed in *Rba. sphaeroides*,[8] and their architecture was more random in *Rhodospirillum photometricum*,[28] *Phaeospirillum molischianum*,[29] *Rhodopseudomonas palustris*,[30] *Rhodobacter blasticus*,[31] and *Rhodobacter veldkampii*,[32] these pigment−protein complexes were all tightly packed within the visualized domains with little or no room for other proteins. Accordingly, neither the cytochrome bc_1 nor ATP synthase complexes were observed in any of these images and, instead, are thought to be localized in the adjacent CM or in ICM regions that are separated from the flat regions adhering to the mica surface that are revealed by AFM. Thus, in contrast to previous models in which the RC−LH1core and bc_1 proteins were thought to be adjacent and form part of supercomplexes,[33] the reality appears to be a considerable separation between individual core and bc_1 complexes, amounting to distances of hundreds of angstroms. How then are UQ molecules able to traverse such long distances to account for the rapid RC electron transfer turnover rates of a few milliseconds or less?

It is expected that transfer of ubuquinol from the RC to the bc_1 complex occurs via lateral diffusion from the RC Q_B site within the cytoplasmic half of the ICM bilayer and "flip-flop" translocation to reach the Q_P site of the bc_1 complex located within the periplasmic monolayer. Thus, transfer of ubiquinone from the bc_1 Q_P site back to the RC Q_B site would involve flip-flop translocation from the periplasmic to the cytoplasmic monolayers followed by diffusion to the empty Q_B site, where it is first reduced to a semiquinone anion and then doubly reduced to a ubiquinol molecule as result of gating of two electrons from the Q_A site and picking up two protons from the cytoplasm. During the movement of UQ in the bilayer, UQ exchanges with the UQ pool.[34] It has recently been shown by ^{2}H NMR[35] that the redox state of the UQ within the pool controls localization of redox species within the bilayer, with the oxidized pool species being located at the bilayer center, while a considerable proportion of the reduced species spans the bilayer through more extensive interaction with phospholipid acyl chains. These localizations are consistent with the roles for the UQ pool in the Q-cycle mechanism of proton and electron flow in the bc_1 complex.[36]

A pathway for quinone diffusion has recently been suggested from an analysis of high-resolution AFM images obtained over the entire surface of *Rsp. photometricum* chromatophores by Liu et al.[37] It was proposed that RC−LH1 core complexes influence their molecular environment within a critical radius of ∼250 Å, in

which a size mismatch was found when seven LH2 complexes surround the core. Within this arrangement, a single lipid membrane space between LH1 and the LH2 rings was observed that could provide sufficient space for quinone diffusion. Such arrays of LH2 and RC−LH1 core complexes formed a network throughout the entire chromatophore for quinone diffusion pathways that may speed the transfer of redox energy to distant cytochrome bc_1 complexes.

In previous work with *Rsp. photometricum* chromatophores, it has been proposed from time-lapse AFM studies and Monte Carlo simulations that short-range corralled diffusion can occur in disordered, more fluid ICM regions containing both LH2 and core complexes.[38] This was proposed to be sufficient to permit flow of ubiquinol between the complexes, once it has exited from the RC Q_B site and escaped through the surrounding LH1 annulus. Thereafter, the rate of long-range flow of metabolically active ubiquinol would be augmented by apparent exclusion from large ordered fields of static LH2 antenna tightly packed with LH2 rings in protein−protein contact; however, this proposal is contrary to the direct effect of LH2 on the slowing of RC electron transfer turnover rates observed here (Figures 3F). Because of the density of disordered domains of mixed complexes within the *Rsp. photometricum* ICM, relatively high turnover rates would be maintained for cytochrome bc_1 and core complexes in sufficient proximity. In *Psp. molischianum*, which like *Rsp. photometricum* also forms a stacked, disklike ICM, a slow quinol diffusion time from the RC to the bc_1 complex of ~260 ms was observed.[39] This was >20-fold slower than that measured for *Rba. sphaeroides*, in which the ICM with a highly organized and ordered arrangement of LH and RC complexes[8−10] assumes a vesicular form.[17]

Accordingly, a different picture of UQ migration has emerged from the AFM topographs of *Rba. sphaeroides*, in which a limited lateral mobility of pigment−protein complexes was observed during repeated AFM scanning of ICM patches.[8] While in these single-membrane bilayer patches, integral membrane protein diffusion could be impeded by interactions with the mica surface, it was nevertheless suggested that lateral migration of individual components may be restricted by the close packing of LH complexes. In contrast to the interpretation of AFM topographs obtained with *Rsp. photometricum* in which LH2 rings were thought to be in protein contact,[38] a recent AFM analysis of LH2-only *Rba. sphaeroides* membranes demonstrated that the shortest distances observed between B850 BChl rings of 3.8 nm provide sufficient room for phospholipid molecules between individual LH2 complexes.[40] This was thought to be adequate for diffusion and shuttling of UQ to foster the efficient flow of cyclic electrons between the RC−LH1 core and physically remote cytochrome bc_1 complexes, possibly via a channeling mechanism.[40] In our studies, in which a correlation between the slowing of electron transport turnover rates and the formation of the LH2 antenna was observed, it seems more likely that this kinetic phenomenon arises from a crowding effect imposed by constraints on UQ flow as the growing ICM bilayer becomes packed with accumulating LH2 complexes or is related to an increased distance between the RC and bc_1 complexes in the expanding ICM.

An alternative possibility is that the slowing of the RC electron transfer turnover rate could arise from limitations in the size of the UQ pool as the cells adapt to reduced light intensity; however, this is unlikely because previous UQ pool size measurements gave values of 24−25 UQs per RC for cells grown to an OD_{660} of 3−4 at 20 W/m^2 and 16 UQs per RC for cells grown to an OD_{660} of 1.4 at a higher light intensity.[34] These values are well in excess of the number of UQs needed to fill the Q_B site of the RC and the Q_N and Q_P sites of the cytochrome bc_1 complex and, in both cases, constitute a substantial UQ pool. Preliminary UQ measurements of petroleum ether extracts of chromatophores by HPLC[41] in this study have given rise to a mean value of 18.9 ± 7.7 UQs/RC (moles per mole) for chromatophore preparations isolated after adaptation from high to low illumination levels for 1, 3, 6, 16, and 36 h. Therefore, the correlation between the slowing of electron transfer turnover and increases in the functional absorption cross section during adaptation to low and diffuse light intensity is interpreted to represent a partial blockage in lateral UQ movement between the RC and bc_1 complexes by the close packing of LH2 rings in expanding LH2-only domains. This would also be expected to increase the functional distance between the RC and cytochrome bc_1 complexes.

Adaptation to Indirect Diffuse Illumination Results in a Stress Response That Alters Protein Levels and Composition. Because the appearance of the chaperonin GroEL and a universal stress protein in CNE gel bands from the UPB indicated that the cells had undergone stress in adapting to growth under indirect diffuse light, it seemed possible that the gradual slowing of RC electron transport might be a reflection of the challenged viability arising as a result of this compromised physiology. Clearly, this is not the case, because a comparable and gradual slowing of RC electron transfer turnover has been demonstrated in steady-state cells undergoing induction of ICM formation after a switch to a low level of aeration in which a parallel expansion of the functional absorption cross section occurs.[13] This is also observed in unstressed cells that expand their functional absorption cross section during adaptation from high illumination levels (1100 W/m^2) to a lower light intensity of 100 W/m^2 (Table 1).

GroEL (cpn60, Hsp60), first identified in *Rba. sphaeroides* by Watson et al.[42] and Terlesky and Tabita,[43] is a group I chaperonin, present in both bacteria and organelles of endosymbiotic origin.[44] As a heat-shock protein, GroEL counteracts stress-induced protein denaturation and assists in the folding of nascent proteins while maintaining preexisting proteins in stable conformations that prevent their aggregation when the proteins are exposed to stress. GroEL forms a double-ring cylinder with a central cavity in which entrapped non-native polypeptides bind and eventually reach their folded states, typically requiring ATP hydrolysis.[44] The double-barreled cochaperonin GroES is required for ejection of the protein from its binding site and enclosure in the central chamber for folding.[45] In *Rba. capsulatus*, GroEL has been shown to be involved in the folding of newly synthesized LH1 polypeptides for stable assembly of the LH1 complex.[46]

The universal stress protein UspA, which has been extensively characterized in *Escherichia coli*, undergoes enhanced expression under conditions of challenged viability, including starvation for nutrients, heat shock, damage to DNA, and osmotic and oxidative stress.[47] UspA is a serine/threonine phosphoprotein that undergoes autophosphorylation specifically in response to arrested growth.[48] *uspA* mutants are impaired in their ability to respond to viability challenges that result in growth arrest, while inactivation or overexpression of *uspA* results in global alterations in the timing of gene expression. The appearance of a 29.9 kDa Usp in the proteomic profile of the CNE gel bands of the UPB isolated from *Rba. sphaeroides* during the terminal stages of adaptation to growth under indirect diffuse illumination, along with extremely high levels of GroEL, has indicated that these

conditions for remodeling of the ICM can be added to the list of stressful growth challenges.

The high spectral counts for the F_1F_O-ATPase subunits were surprising, given the relatively low abundance of the ATPase reported for chromatophores[49,50] together with the inability to detect this coupling factor or the more abundant cytochrome bc_1 complex in AFM.[8] In this connection, the high levels of these ATPase subunits together with those of the bc_1 complex apparently associated with the LH2-enriched fractions are consistent with the possibility noted above, which places these components at ICM vesicle edges, thought to contain LH2-only domains, that are outside the flat ICM vesicle regions revealed by AFM. In high-light chromatophores, in which levels of LH2 are very low,[12] the F_1 particle has been shown by Western blotting and activity staining to migrate to the exact position normally occupied by the upper intermediate (LH2−LH1) band (unpublished data; this is also reflected in the UPB as seen in Figure S1B of the Supporting Information), so that the appearance of ATPase in this band when LH2 levels are higher cannot be ascribed to an in vivo association with the antennae. On the other hand, the high ATPase counts in the chromatophore bottom (LH2) band (Figure 4C) may reflect an in vivo association between ATPase and LH2-only domains that existed in the membrane. The relatively high levels of cytochrome bc_1 in the LH2 band of chromatophores [4% of total spectral counts (Figure S2A of the Supporting Information) as compared to 2% in the LH1−LH2 band (Figure S2B of the Supporting Information)] may also reflect an authentic association with LH2, further supporting the notion that these complexes are located in membrane domains outside the regions scanned by AFM. Another important finding from the proteomic analysis was the high level of energy transduction-coupled oxidoreductases and transport proteins in the chromatophore and UPB gel bands. These findings are consistent with a limited CM invagination under diffuse light illumination conditions in which ICM vesicles may remain attached to the ICM continuum[17] and the confirmation that the UPB membranes are of CM origin, from the relatively high levels of these two protein clusters in the UPB gel bands.

■ ASSOCIATED CONTENT

Supporting Information. Bar graphs (Figure S1) and pie charts (Figures S2 and S3), showing the distributions of clusters of orthologous groups detected in the proteomic analysis of gel bands. This material is available free of charge via the Internet at http://pubs.acs.org.

■ AUTHOR INFORMATION

Corresponding Author

*Phone: (732) 445-3985. Fax: (732) 445-4213. E-mail: rniederm@rci.rutgers.edu.

Notes

[a]The photosystem of *Rba. sphaeroides* consists of the LH2 peripheral and LH1−RC core complexes, the cytochrome bc_1 complex, and cytochrome c_2. The transfer of excitations from the LH complexes to the RC−BChl special pair initiates a charge separation, resulting in the formation of ubiquinol at the RC−Q_B site. After entering the UQ pool, a ubiquinol drives electron flow through the cytochrome bc_1 complex. After an electron is transferred to cytochrome c_2, the ferrocytochrome serves as donor to the photooxidized RC−BChl special pair, thereby completing the cycle of electron flow.

Present Addresses

[†]Department of Physics and Astronomy, Faculty of Sciences, Vrije Universiteit, De Boelelaan 1081, 1081 HV Amsterdam, The Netherlands.

Funding Sources

Supported by U.S. Department of Energy Grant DE-FG02-08ER15957 from the Chemical Sciences, Geosciences and Biosciences Division, Office of Basic Energy Sciences, Office of Science, and the Aresty Research Center for Undergraduates at Rutgers University.

■ ACKNOWLEDGMENT

We thank Oluwatobi B. Olubanjo for assistance with membrane purification procedures and Prof. Peter Lobel and Dr. Haiyan Zheng of the Center for Advanced Biotechnology and Medicine (University of Medicine and Dentistry of New Jersey, Piscataway, NJ) for conducting the proteomic analysis.

■ ABBREVIATIONS

BChl, bacteriochlorophyll *a*; FRR, fast repetition rate; F_M, maximal fluorescence yield; F_0, minimal fluorescence yield; F_V, variable fluorescence ($F_M - F_0$); CM, cytoplasmic membrane; ICM, intracytoplasmic membrane; LH1, dimeric core light-harvesting complex, consisting of paired elliptical arrangements of 14 BChl dimers absorbing at 875 nm; LH2, peripheral light-harvesting complex, containing BChl rings of nine monomeric and nine dimeric BChls, absorbing at 800 and 850 nm, respectively; Q_A, reaction center primary ubiquinone site; Q_B, reaction center secondary ubiquinone site; RC, photochemical reaction center; *p*, antenna connectivity; σ, functional absorption cross section; τ_{QA}, time constant for electron transport on the acceptor side of the reaction center (Q_A reoxidation); τ_{Qpool}, time constant for the transport of electrons to the cytochrome bc_1 complex (reoxidation of the Q pool); TEM, transmission electron microscopy; UPB, upper-pigmented band; UQ, ubiquinone$_{10}$ and ubiquinol$_{10}$ redox species.

■ REFERENCES

(1) Hunter, C. N., Daldal, F., Thurnauer, M. C., and Beatty, J. T., Eds. (2008) *The Purple Phototrophic Bacteria. Advances in Photosynthesis and Respiration*, Vol. 28, Springer, Dordrecht, The Netherlands.

(2) Sturgis, J. N., and Niederman, R. A. (2008) Organization and Assembly of Light-Harvesting Complexes in the Purple Bacterial Membrane. In *The Purple Phototrophic Bacteria. Advances in Photosynthesis and Respiration* (Hunter, C. N., Daldal, F., Thurnauer, M. C., and Beatty, J. T., Eds.) Vol. 28, pp 253−273, Springer, Dordrecht, The Netherlands.

(3) Drews, G., and Golecki, J. R. (1995) Structure, Molecular Organization, and Biosynthesis of Membranes of Purple Bacteria. In *Anoxygenic Photosynthetic Bacteria* (Blankenship, R. E., Madigan, M. T., and Bauer, C. E., Eds.) pp 231−257, Kluwer Academic Publishers, Dordrecht, The Netherlands.

(4) Monger, T. G., and Parson, W. W. (1977) Singlet-triplet fusion in *Rhodopseudomonas spheroides* chromatophores. A probe of the organization of the photosynthetic apparatus. *Biochim. Biophys. Acta 460*, 393–407.

(5) Bakker, J. G. C., van Grondelle, R., and den Hollander, W. T. F. (1983) Trapping, loss and annihilation of excitations in a photosynthetic

system. II. Experiments with the purple bacteria *Rhodospirillum rubrum* and *Rhodopseudomonas capsulata*. *Biochim. Biophys. Acta 725*, 508–518.

(6) Hunter, C. N., Kramer, H. J. M., and van Grondelle, R. (1985) Linear dichroism and fluorescence emission of antenna complexes during photosynthetic unit assembly in *Rhodopseudomonas sphaeroides*. *Biochim. Biophys. Acta 807*, 44–51.

(7) Vos, M., van Grondelle, R., van der Kooij, F. W., van de Poll, D., Amesz, J., and Duysens, L. M. N. (1986) Singlet-singlet annihilation at low temperatures in the antenna of purple bacteria. *Biochim. Biophys. Acta 850*, 501–512.

(8) Bahatyrova, S., Frese, R. N., Siebert, C. A., Olsen, J. D., van der Werf, K. O., van Grondelle, R., Niederman, R. A., Bullough, P. A., Otto, C., and Hunter, C. N. (2004) The native architecture of a photosynthetic membrane. *Nature 430*, 1058–1062.

(9) Sturgis, J. N., and Niederman, R. A. (2008) Atomic force microscopy reveals multiple patterns of antenna organization in purple bacteria: Implications for energy transduction mechanisms and membrane modeling. *Photosynth. Res. 95*, 269–278.

(10) Sturgis, J. N., Tucker, J. D., Olsen, J. D., Hunter, C. N., and Niederman, R. A. (2009) Atomic force microscopy studies of native photosynthetic membranes. *Biochemistry 48*, 3679–3698.

(11) Frese, R. N., Siebert, C. A., Niederman, R. A., Hunter, C. N., Otto, C., and van Grondelle, R. (2004) The long-range organization of a native photosynthetic membrane. *Proc. Natl. Acad. Sci. U.S.A. 101*, 17994–17999.

(12) Woronowicz, K., and Niederman, R. A. (2010) Proteomic analysis of the developing intracytoplasmic membrane in *Rhodobacter sphaeroides* during adaptation to low light intensity. *Adv. Exp. Med. Biol. 675*, 161–178.

(13) Koblízek, M., Shih, J. D., Breitbart, S. I., Ratcliffe, E. C., Kolber, Z. S., Hunter, C. N., and Niederman, R. A. (2005) Sequential assembly of photosynthetic units in *Rhodobacter sphaeroides* as revealed by fast repetition rate analysis of variable bacteriochlorophyll *a* fluorescence. *Biochim. Biophys. Acta 1706*, 220–231.

(14) Niederman, R. A., Mallon, D. E., and Parks, L. C. (1979) Membranes of *Rhodopseudomonas sphaeroides*. VI. Isolation of a fraction enriched in newly synthesized bacteriochlorophyll *a*-protein complexes. *Biochim. Biophys. Acta 555*, 210–220.

(15) Niederman, R. A. (2006) Structure, Function and Formation of Bacterial Intracytoplasmic Membranes. In *Complex Intracellular Structures in Prokaryotes. Microbiology Monographs* (Shively, J. M., Ed.) Vol. 2, pp 193−227, Springer-Verlag, Berlin.

(16) Niederman, R. A. (2010) MicroCommentary: Eukaryotic behaviour of a prokaryotic energy transducing membrane: Fully detached vesicular organelles arise by budding from the *Rhodobacter sphaeroides* intracytoplasmic photosynthetic membrane. *Mol. Microbiol. 76*, 803–805.

(17) Tucker, J. D., Siebert, C. A., Escalante, M., Adams, P. G., Olsen, J. D., Otto, C., Stokes, D. L., and Hunter, C. N. (2010) Membrane invagination in Rhodobacter sphaeroides is initiated at curved regions of the cytoplasmic membrane, then forms both budded and fully detached spherical vesicles. *Mol. Microbiol. 76*, 833–847.

(18) Hunter, C. N., Tucker, J. D., and Niederman, R. A. (2005) The assembly and organisation of photosynthetic membranes in *Rhodobacter sphaeroides*. *Photochem. Photobiol. Sci. 4*, 1023–1027.

(19) Kolber, Z. S., Prasil, O., and Falkowski, P. G. (1998) Measurements of variable chlorophyll fluorescence using fast repetition rate techniques: Defining methodology and experimental protocols. *Biochim. Biophys. Acta 1367*, 88–106.

(20) Cohen-Bazire, G., Sistrom, W. R., and Stanier, R. Y. (1956) Kinetic studies of pigment synthesis by non-sulfur purple bacteria. *J. Cell. Comp. Physiol. 49*, 25–68.

(21) Wittig, I., Karas, M., and Schägger, H. (2007) High resolution clear native electrophoresis for in-gel functional assays and fluorescence studies of membrane protein complexes. *Mol. Cell. Proteomics 6*, 1215–1225.

(22) Papagiannakis, E., Kennis, J. T. M., van Stokkum, I. H. M., Cogdell, R. J., and van Grondelle, R. (2002) An alternative carotenoid-to-bacteriochlorophyll energy transfer pathway in photosynthetic light harvesting. *Proc. Natl. Acad. Sci. U.S.A. 99*, 6017–6022.

(23) Sturgis, J. N., Hunter, C. N., and Niederman, R. A. (1988) Spectra and extinction coefficients of near-infrared absorption bands in membranes of *Rhodobacter sphaeroides* mutants lacking light-harvesting and reaction center complexes. *Photochem. Photobiol. 48*, 243–247.

(24) Tatusov, R. L., Koonin, E. V., and Lipman., D. J. (1997) A genomic perspective on protein families. *Science 278*, 631–637.

(25) Hunter, C. N., Pennoyer, J. D., Sturgis, J. N., Farrelly, D., and Niederman, R. A. (1988) Oligomerization states and associations of light-harvesting pigment-protein complexes of *Rhodobacter sphaeroides* as analyzed by lithium dodecyl sulfate-polyacrylamide gel electrophoresis. *Biochemistry 27*, 3459–3467.

(26) Sturgis, J. N., and Niederman, R. A. (1996) The effect of different levels of the B800−850 light-harvesting complex on intracytoplasmic membrane development in *Rhodobacter sphaeroides*. *Arch. Microbiol. 165*, 235–242.

(27) Scheuring, S., Levy, D., and Rigaud, J. L. (2005) Watching the components of photosynthetic bacterial membranes and their in situ organisation by atomic force microscopy. *Biochim. Biophys. Acta 1712*, 109–127.

(28) Scheuring, S., and Sturgis, J. N. (2005) Chromatic adaptation of photosynthetic membranes. *Science 309*, 484–487.

(29) Gonçalves, R. P., Bernadac, A., Sturgis, J. N., and Scheuring, S. (2005) Architecture of the native photosynthetic apparatus of *Phaeospirillum molischianum*. *J. Struct. Biol. 152*, 221–228.

(30) Scheuring, S., Gonçalves, R. P., Prima, V., and Sturgis, J. N. (2006) The photosynthetic apparatus of *Rhodopseudomonas palustris*: Structures and organization. *J. Mol. Biol. 358*, 83–96.

(31) Scheuring, S., Busselez, J., and Lévy, D. (2005) Structure of the dimeric PufX-containing core complex of *Rhodobacter blasticus* by in situ atomic force microscopy. *J. Biol. Chem. 280*, 1426–1431.

(32) Liu, L.-N., Sturgis, J. N., and Scheuring, S. (2010) Native architecture of the photosynthetic membrane from *Rhodobacter veldkampii*. *J. Struct. Biol. 173*, 138–145.

(33) Joliot, P., Joliot, A., and Verméglio, A. (2005) Fast oxidation of the primary electron acceptor under anaerobic conditions requires the organization of the photosynthetic chain of *Rhodobacter sphaeroides* in supercomplexes. *Biochim. Biophys. Acta 1706*, 204–214.

(34) Venturoli, G., Fernández-Velasco, J. G., Crofts, A. R., and Melandri, B. A. (1986) Demonstration of collisional interaction of ubiquinol with the ubiquinol-cytochrome c_2 oxidoreductase complex in chromatophores from *Rhodobacter sphaeroides*. *Biochim. Biophys. Acta 851*, 340–352.

(35) Ausili, A., Torrecillas, A., Aranda, F., de Godos, A., Sánchez-Bautista, S., Corbalán-García, S., and Gómez-Fernández, J. C. (2008) Redox state of coenzyme Q_{10} determines its membrane localization. *J. Phys. Chem. B 112*, 12696–12702.

(36) Crofts, A. R., and Meinhardt, S. W. (1982) A Q-cycle mechanism for the cyclic electron-transfer chain of *Rhodopseudomonas sphaeroides*. *Biochem. Soc. Trans. 10*, 201–203.

(37) Liu, L.-N., Duquesne, K., Sturgis, J. N., and Scheuring, S. (2009) Quinone pathways in entire photosynthetic chromatophores of *Rhodospirillum photometricum*. *J. Mol. Biol. 393*, 27–35.

(38) Scheuring, S., and Sturgis, J. N. (2006) Dynamics and diffusion in photosynthetic membranes from *Rhodospirillum photometricum*. *Biophys. J. 91*, 3707–3717.

(39) Mascle-Allemand, C., Lavergne, J., Bernadac, A., and Sturgis, J. N. (2008) Organisation and function of the *Phaeospirillum molischianum* photosynthetic apparatus. *Biochim. Biophys. Acta 1777*, 1552–1559.

(40) Olsen, J. D., Tucker, J. D., Timney, J. A., Qian, P., Vassilev, C., and Hunter, C. N. (2008) The organization of LH2 complexes in membranes from *Rhodobacter sphaeroides*. *J. Biol. Chem. 283*, 30772–30779.

(41) Francia, F., Dezi, M., Rebecchi, A., Mallardi, A., Palazzo, G., Melandri, B. A., and Venturoli, G. (2004) Light-harvesting complex 1 stabilizes $P^+Q_A^-$ charge separation in reaction centers of *Rhodobacter sphaeroides*. *Biochemistry 43*, 14199–14210.

(42) Watson, G. M., Mann, N. H., MacDonald, G. A., and Dunbar, B. (1990) Identification and characterization of a GroEL homologue in *Rhodobacter sphaeroides*. *FEMS Microbiol. Lett. 60*, 349–353.

(43) Terlesky, K. C., and Tabita, F. R. (1991) Purification and characterization of the chaperonin 10 and chaperonin 60 proteins from *Rhodobacter sphaeroides*. *Biochemistry 30*, 8181–8186.

(44) Kim, S. Y., Miller, E. J., Frydman, J., and Moerner, W. E. (2010) Action of the chaperonin GroEL/ES on a non-native substrate observed with single-molecule FRET. *J. Mol. Biol. 401*, 553–563.

(45) Clare, D. K., Bakkes, P. J., van Heerikhuizen, H., van der Vies, S. M., and Saibil, H. R. (2009) Chaperonin complex with a newly folded protein encapsulated in the folding chamber. *Nature 457*, 107–110.

(46) Drews, G. (1996) Formation of the light-harvesting complex I (B870) of anoxygenic phototrophic purple bacteria. *Arch. Microbiol. 166*, 151–159.

(47) Nachin, L., Nannmark, U., and Nyström, T. (2005) Differential roles of the universal stress proteins of *Escherichia coli* in oxidative stress resistance, adhesion, and motility. *J. Bacteriol. 187*, 6265–6272.

(48) Freestone, P., Trinei, M., Clarke, S. C., Nyström, T., and Norris, V. (1998) Tyrosine phosphorylation in *Escherichia coli*. *J. Mol. Biol. 279*, 1045–1051.

(49) Feniouk, B. A., Cherepanov, D. A., Voskoboynikova, N. E., Mulkidjanian, A. Y., and Junge, W. (2002) Chromatophore vesicles of *Rhodobacter capsulatus* contain on average one F_OF_1-ATP synthase each. *Biophys. J. 82*, 1115–1122.

(50) Gubellini, F., Francia, F., Turina, P., Lévy, D., Venturoli, G., and Melandri, B. A. (2007) Heterogeneity of photosynthetic membranes from *Rhodobacter capsulatus*: Size dispersion and ATP synthase distribution. *Biochim. Biophys. Acta 1767*, 1340–1352.